Langmuir

Article

pubs.acs.org/Langmuir

Simulated Adhesion between Realistic Hydrocarbon Materials: Effects of Composition, Roughness, and Contact Point

Kathleen E. Ryan,[†] Pamela L. Keating,[†] Tevis D. B. Jacobs,[‡] David S. Grierson,[§] Kevin T. Turner,[∥] Robert W. Carpick,[∥] and Judith A. Harrison*[,†]

[†]Chemistry Department, United States Naval Academy, Annapolis, Maryland 21402, United States

[‡]Department of Materials Science & Engineering, University of Pennsylvania, 3231 Walnut Street, Philadelphia, Pennsylvania 19104, United States

[§]SysteMECH, LLC, Madison, Wisconsin 53705, United States

[∥]Department of Mechanical Engineering & Applied Mechanics, University of Pennsylvania, 220 S. 33rd Street, Philadelphia, Pennsylvania 19104, United States

ABSTRACT: The work of adhesion is an interfacial materials property that is often extracted from atomic force microscope (AFM) measurements of the pull-off force for tips in contact with flat substrates. Such measurements rely on the use of continuum contact mechanics models, which ignore the atomic structure and contain other assumptions that can be challenging to justify from experiments alone. In this work, molecular dynamics is used to examine work of adhesion values obtained from simulations that mimic such AFM experiments and to examine variables that influence the calculated work of adhesion. Ultrastrong carbon-based materials, which are relevant to high-performance AFM and nano- and micromanufacturing applications, are considered. The three tips used in the simulations were composed of amorphous carbon terminated with hydrogen (a-C−H), and ultrananocrystalline diamond with and without hydrogen (UNCD−H and UNCD, respectively). The model substrate materials used were amorphous carbon with hydrogen termination (a-C−H) and without hydrogen (a-C); ultrananocrystalline diamond with (UNCD−H) and without hydrogen (UNCD); and the (111) face of single crystal diamond with (C(111)−H) and without a monolayer of hydrogen (C(111)). The a-C−H tip was found to have the lowest work of adhesion on all substrates examined, followed by the UNCD−H and then the UNCD tips. This trend is attributable to a combination of roughness on both the tip and sample, the degree of alignment of tip and substrate atoms, and the surface termination. Continuum estimates of the pull-off forces were approximately 2−5 times larger than the MD value for all but one tip−sample pair.

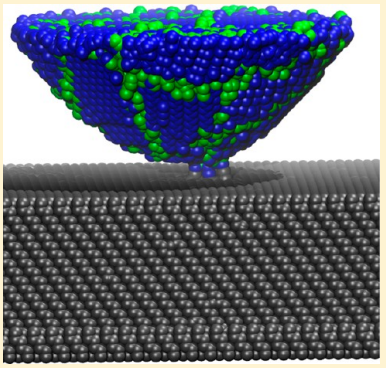

INTRODUCTION

Mechanical properties of materials and interfaces, such as the elastic modulus or the work of adhesion W, are commonly extracted from atomic force microscopy (AFM) experiments by applying continuum mechanics models to experimental data. The choice of model applied depends on the properties of the contact. For example, the Johnson−Kendall−Roberts (JKR),[1] Derjaguin−Müller−Toporov (DMT),[2] and Maugis−Dugdale[3] models can all be used to extract a value of W from measurements of the pull-off force required to separate a paraboloidal tip from a flat substrate. These models have been extended to spherical tips,[4−6] flat-ended indenters,[7,8] and power-law-shaped tips.[9] Extracting W, the work per unit area required to separate two semi-infinite materials from their equilibrium contact separation to infinity, is important because it controls many properties, including the force required to separate the surfaces, the propensity to fracture instead of separate, and the behavior of all of the contact properties (area, deformation, stiffness, and stresses) of single-asperity contacts. Continuum mechanics models that are based on elasticity theory and therefore rely on assumptions about the shape (known geometry), deformation (small strains, contact radius being much smaller than the body radius), and mechanical behavior (isotropic, linear elastic response) are routinely used to analyze AFM data. However, many of the underlying assumptions can break down for nanoscale AFM tips. Therefore, model predictions may contain significant errors, as has been shown using molecular dynamics (MD) simulations of contact tests that utilize simple Lennard-Jones potentials, flat elastic substrates, and spherical nanoscale tips formed from crystalline and amorphous fcc materials.[10,11] That work demonstrated that the atomic-scale roughness present at the surface of a tip composed of discrete atoms produces local stresses, W values, and definition-dependent contact areas that differ by factors of 2 to 4 from continuum predictions. The

Received: November 9, 2013
Revised: January 30, 2014
Published: February 4, 2014

   dx.doi.org/10.1021/la404342d | *Langmuir* 2014, 30, 2028−2037

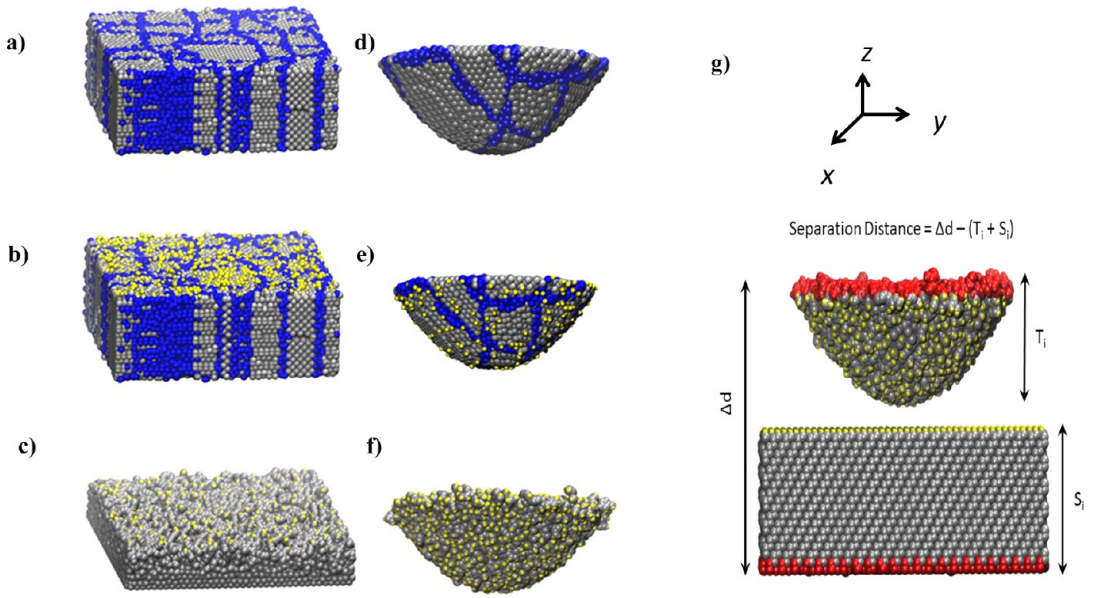

Figure 1. (a) UNCD, (b) UNCD−H, and (c) a-C−H examined in this work. The UNCD, UNCD−H, and a-C−H tips are shown in d−f, respectively. Blue, gray, and yellow spheres represent atoms that define the UNCD grain boundaries, carbon atoms, and hydrogen atoms, respectively. (g) Cartesian coordinate system shown along with the C(111)−H substrate and a-C−H tip used in the MD simulations. Layers held rigid during the simulations are colored red.

smallest deviations from continuum predictions were obtained for dense tips whose atoms formed a nearly continuous sphere.

MD simulations were used here to study the adhesion of paraboloidal tips formed from amorphous carbon ((a-C), a type of diamondlike carbon (DLC)), and ultrananocrystalline diamond (UNCD) on substrates of UNCD, a-C, and single-crystal diamond. Many types of DLC, including a-C, have already been demonstrated as effective wear-resistant coatings, and they are in widespread use in commercially available devices.[12,13] UNCD contains many of the desirable properties of single-crystal diamond (hardness, inertness, and wear resistance) and can be deposited as a conformal thin film.[14,15] Both UNCD and DLC have demonstrated utility as tip materials for AFM probes[16,17] and other devices with nanoscale components.[14,17−20]

METHOD

To facilitate the comparison of the simulated and AFM force-curve data, the simulations were designed to match the conditions of AFM experiments within computational constraints. The choice of materials was guided by their availability for experiments. Paraboloidal tips, such as those used in AFM experiments,[9,21] were created from a-C and UNCD and were subsequently terminated with H; these are denoted as a-C−H and UNCD−H tips. In addition, a UNCD tip was also tested.

The three tips were each brought into contact with six different substrates: diamond (111) (with 1 × 1 surface termination) with and without H termination (designated C(111) and C(111)−H, respectively), an a-C film with and without H (again, designated as a-C and a-C−H, respectively), and ultrananocrystalline diamond with and without H termination (UNCD and UNCD−H, respectively). Our a-C−H film should not be confused with hydrogenated amorphous carbon, commonly denoted in the literature as a-C:H; such a film has hydrogen incorporated throughout the entire film, not just on the surface as it does here. Hydrogen-terminated (H-terminated) surfaces are included in this analysis to approximate realistic materials that are either deliberately H-terminated at the end of their growth or would be often exposed to air.[22,23] With air exposure, reactive bulk-terminated surfaces will quickly react with ambient species such as oxygen or hydrogen to form a passivation layer. Modeling oxygen species requires the use of a modified potential[24,25] and will be considered in future work.

Chemical or physical vapor deposition techniques are used to make a-C films, where the technique and the deposition process control the structure of the film.[12,26] Two widely used simulation methods for creating simulated a-C films, which are computationally efficient, are the homogeneous condensation of a vapor and ultrafast quenching of liquid carbon.[27−30] The a-C substrates used here were created using the latter approach. A diamond substrate was melted by heating to 8000 K for 10.0 ps using a Langevin thermostat[31] and then quenched to 0 K in 10.0 ps. After being quenched, the a-C substrates were brought to 300 K by heating in 100 K increments of 10 ps each. The resulting a-C substrate contains approximately 1% overcoordinated carbon, found mostly on the surface of the a-C. The surface of the a-C substrate was H-terminated to produce a-C−H by placing the substrate in an atmosphere of atomic H at 300 K, which reduces the amount of, but does not completely eliminate, under-coordinated carbon. The a-C−H substrate contains 9.8% sp^3, 80.1% sp^2, 9.8% sp, and approximately 0.3% overcoordinated carbon.

UNCD substrates were modeled using columnar nanostructured materials created by placing diamond (111) or (001) crystallites into four-sided columns with randomly created shapes. Grain boundaries between the diamond regions were created by heating atoms that were within 0.2 nm of the shape edges to 8000 K, while the atoms belonging to the grains were held fixed and subsequently cooled. These substrates have grain sizes of 2−4 nm and amorphous carbon grain boundaries approximately 0.2 nm wide, similar to what is observed experimentally for UNCD.[14,15,32,33] The diamond grains extend through the depth of the sample, creating a 2D columnar sample (Figure 1a,b). UNCD samples with structures analogous to these columnar substrates have been observed experimentally.[34] They were H-terminated in the way described above to form UNCD−H. For comparison, single-crystal C(111)(1 × 1) and C(111)(1 × 1)−H substrates were also examined. Details regarding the substrate and tip sizes are given in Table 1.

Axisymmetric, parabolic tips were formed from cubic samples of UNCD and a-C using a radius of curvature, *R*, of 2.5 nm (Figure 1d−f). Shaping the tips from the larger samples leaves unsaturated carbon atoms on the surfaces of the tips. These "freshly cleaved" tips

dx.doi.org/10.1021/la404342d | *Langmuir* 2014, 30, 2028−2037

Table 1. Simulation Details

surface name	atoms (C:H)	x (nm)	y (nm)	z (nm)	rms roughness (nm)
C(111)	66 240:0	10.1	10.4	3.6	0.011
C(111)−H	64 400:1840	10.1	10.4	3.6	0.012
UNCD	64 783:0	10.1	10.4	4.2	0.0487
UNCD−H	64 782:259	10.1	10.4	4.3	0.056
a-C	23 703:0	9.8	11.4	2	0.131
a-C−H	23 701:277	9.8	11.4	2	0.135
tip	atoms (C:H)	x (nm)	y (nm)	z (nm)	R (nm)
a-C−H	9923:1256	8	7.8	3.5	2.5
UNCD	13 806:0	8	8	3.4	2.5
UNCD−H	13 814:234	8	8	3.5	2.5

The x and y values for tips are specified at their widest point.

were placed in an atmosphere of atomic H at 300 K to H-terminate them.

The adaptive intermolecular reactive empirical bond-order (AIREBO) potential[35] and the large-scale atomic/molecular massively parallel simulator (LAMMPS)[36] were used to carry out the MD simulations. The AIREBO potential contains covalent bonding terms, including torsional effects, and intermolecular terms.

Force-curve simulations were performed by holding the outer portions of the tip and the substrate rigid (Figure 1g), whereas Newton's equations of motion were integrated for the remaining atoms. The time step was 0.25 fs. The simulation was maintained at 300 K by applying a Langevin thermostat to thin regions (approximately 0.5 nm thick for the UNCD and C(111) substrates and 0.3 nm thick for the a-C substrate) adjacent to the rigid layers but far from the contacting surfaces. The rigid tip atoms were moved at a constant velocity (0.05 nm/ps) toward and away from the substrate to bring the tip and substrate into and out of contact, respectively.

Because the forces on the rigid-layer atoms are closely correlated to what is measured in an AFM experiment, these forces are commonly used to construct simulated load versus separation curves. The rigid-layer forces provide only an indirect picture of the dynamics occurring at the contacting interface.[37] Contact force refers to the net force exerted by the entire set of tip atoms on some subset of the sample atoms, with the smallest subset being a single atom, which is referred to as the atomic-contact force. The atomic-contact force on a single substrate atom would include only force contributions from tip atoms and would not include forces exerted by the remaining sample atoms. This differs from the net force on the substrate atom (needed to evolve the dynamics), which includes forces exerted by all other substrate atoms. Summing the contact forces from all sample atoms gives the all-atom force exerted by the tip on the sample, which is equivalent to the net force on the rigid layers. Because the tip and substrate are in mechanical equilibrium, the total forces are equal and of opposite sign. The load versus separation curves can be calculated through either the average net force on the rigid-layer atoms or by using the sum of contact forces on all atoms from the tip. Contact forces are used here because they provide the same information as the rigid-layer forces and they can provide additional insight into specific atomic interactions at the interface.[37] The total contact force on the tip atoms in the z direction was averaged every 400 time steps or every 0.005 nm. Herein, the tip−sample separation is defined for the simulated systems using the equation $\Delta d - (T_i + S_i)$, where Δd is the separation between the outermost layers of the tip and sample, T_i is the initial vertical extent of the tip, and S_i is the initial thickness of the substrate (Figure 1g). This definition of distance effectively corresponds to the approach distance measured from distant points in continuum bodies along the z axis; it would be equal to zero if the outermost tip and substrate atoms were to have the same vertical (z) position and no interaction forces were acting. The finite value of this separation when the net interaction force is zero represents the equilibrium separation of the bodies. This variable does not reflect the elastic deformations of the tip or substrate. As such, it also represents the relative z motion of the cantilever−substrate during force-separation experiments. A configuration with a repulsive load of approximately 10 nN was used as a starting point to reverse the tip motion. Periodic boundary conditions were applied in the x and y directions (Figure 1g).

RESULTS AND DISCUSSION

Dependence of Adhesion Force Measurements on the Tip and Substrate. AFM measurements of tip−sample interactions are typically represented in the form of a force curve, which is a plot of the normal force on the tip versus the separation distance. The pull-off force is obtained from these curves and is directly related to the W value between the tip and substrate. Force curves were generated for all of the tip−substrate pairs in the simulations. Curves were observed both with and without hysteresis. Plots of contact force on a UNCD tip as it approaches two nominally flat, H-terminated substrates are shown as a function of the tip−sample separation in Figure 2a,b. No hysteresis occurs, and only intermolecular (van der Waals) interactions occur between all tip and substrate atoms; no covalent bonds form. In contrast, force curves between the UNCD tip and either C(111) or UNCD (Figure 2c,d) exhibited hysteresis, which was the result of covalent bonds forming between the tip and sample. Although small attractive contributions to the force occur when these bonds form, much larger forces are required to separate them. The force relaxations seen upon retraction in Figure 2c,d are specifically associated with the breaking of covalent C−C bonds. No hysteresis was observed when the UNCD−H, the a-C−H, and the UNCD tips interacted with H-terminated substrates.

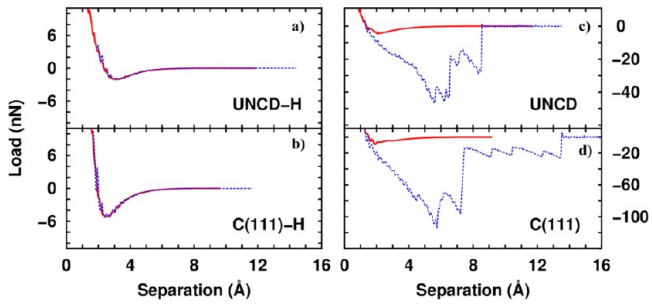

Figure 2. Force curves comparing indent (red) and pull-back (blue) simulations of the UNCD tip. Hydrogen-terminated substrates are shown in a and b, and non-hydrogen-terminated substrates are shown in c and d. Substrate identities are given in the legend.

AFM force-curve measurements typically show additional hysteresis because of the finite stiffness of the cantilever, which leads to snap-in and pull-off instabilities when the gradient of the tip−sample force exceeds the cantilever spring constant. In experiments, the pull-off force F_{po} is the minimum force (maximum attractive force) needed to separate the tip from the sample. The minimum in the approach portion of the force curve is nearly equal to F_{po} when there is a lack of hysteresis in the simulated force curves (Figure 2a,b).[38] In the cases where hysteresis is present, F_{po} is not equal to the minimum in the approach portion of the force curve. So that all tip−substrate pairs can be compared, the minimum in the simulated approach curves is used here and is referred to as the adhesion force, F_{adh}.

In AFM experiments, multiple force curves are typically obtained to check the variability associated with F_{po} for a given tip−substrate pair. Similarly, error bars can be generated by

dx.doi.org/10.1021/la404342d | Langmuir 2014, 30, 2028−2037

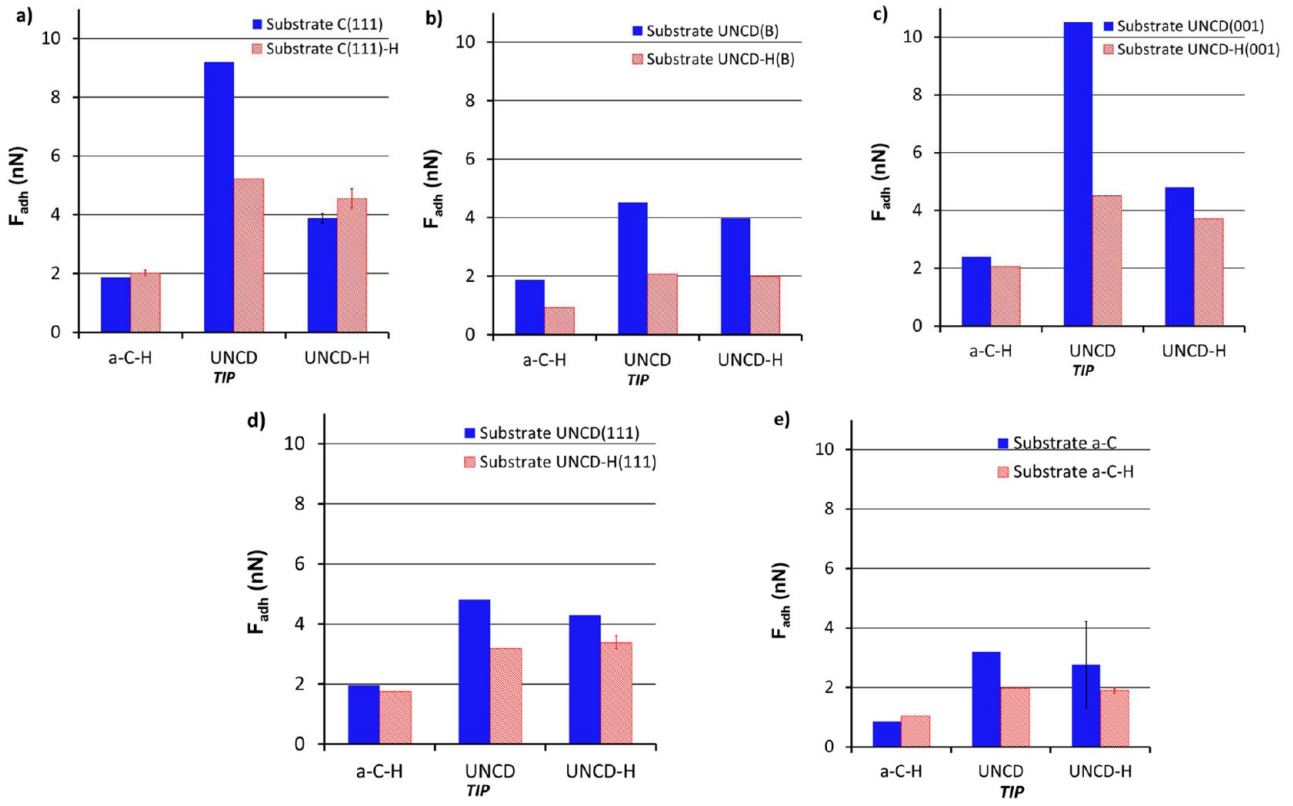

Figure 3. Adhesive force (F_{adh}) taken as the minimum in the force curve for all tip−substrate combinations. The identity of the substrates is given in the legend. Blue solid and red cross-hatched bars represent non-hydrogen-terminated and hydrogen-terminated substrates, respectively. UNCD(B), UNCD(001), and UNCD(111) indicate that in separate simulations a given tip impacts the boundary between the diamond grain and the (001) and (111) grains, respectively. The tip identity is shown along the x axis. Error bars in a, d, and e represent the positive standard deviation for five different contact points.

performing multiple simulations of force curves with tips translating some fraction of a unit cell distance. Repeated force-curve simulations using both UNCD−H and a-C−H tips against C(111)−H substrates produced variations in F_{adh} of approximately 7.2 and 5.0%, respectively.[21] Roughening the tip was also shown to increase the variability of F_{adh} markedly while significantly reducing its mean value.[21] Multiple force curves with the tip shifted a fraction of the substrate unit-cell length were generated for several of the tip−substrate pairs, and the standard deviations associated with F_{adh} are used to generate the error bars (Figure 3). The uncertainty associated with F_{adh} for other tip−sample pairs is assumed to be approximately the same magnitude; on the basis of prior simulations, these are unlikely to be larger than 10%.

When the substrate has a heterogeneous structure (e.g., UNCD), another factor that can cause variation in F_{adh} between force curves is the contact point of the tip with respect to the substrate. All of the tips were brought into contact at three different locations on the UNCD substrates: on the (111) or (001) surface of a grain (designated UNCD−H(111) or UNCD−H(001), respectively, or on a grain boundary (designated UNCD−H(B)). The UNCD tips were chosen to have a (111) grain at their apex. These tips are oriented so that the $[1\bar{1}0]$ and the $[11\bar{2}]$ directions correspond to the x and y Cartesian axes, respectively. Because the tip apex is 3 to 4 times smaller than most (111) and (001) UNCD grains, it can be positioned so that the contact zone falls completely within either grain. The (111) grain where the tip makes contact is also oriented with the $[1\bar{1}0]$ and $[11\bar{2}]$ directions along x and y, respectively. The surface order on the (111) grain is disrupted slightly by terminal carbon atoms "bending" to bond with other unsaturated surface carbons. In the initial conformation, the terminal carbon atoms on the tip and (111) grain are not directly above and below one another. The $[\bar{1}10]$ and [110] directions on the (001) substrate grain where tip contact is made are at approximately 45° with respect to the x and y axes. Thus, the x axis corresponds to the [010] direction. Values of F_{adh} for all tip−substrate combinations, including the three locations on the UNCD substrate, are shown in Figure 3.

The value of F_{adh} is affected by the choice of tip and substrate material, the surface termination, the substrate roughness, and the specific contact point on the substrate (Figure 3). The a-C−H tip exhibited the lowest values of F_{adh} for all 10 substrates examined, and the unpassivated UNCD tip had the largest values of F_{adh} on all 10 substrates (although values are within 10%).

In all except three cases, terminating the substrate with H lowers F_{adh} (Figure 3). For example, F_{adh} is higher when the UNCD−H tip is brought into contact on any location on the unpassivated UNCD compared to the values obtained on the UNCD−H substrates (Figure 3b−d). Although F_{adh} is incrementally larger on the C(111)−H surface than is C(111) when both the UNCD−H and the a-C−H tips are used (Figure 3a), F_{adh} values measured on the C(111)−H and the C(111) surfaces with the UNCD−H tip (Figure 3a) are statistically equivalent. Large values of F_{adh} can be obtained when both the tip and the substrate lack H termination, as seen when the UNCD tip contacts and the C(111) (Figure 3a) or

dx.doi.org/10.1021/la404342d | Langmuir 2014, 30, 2028−2037

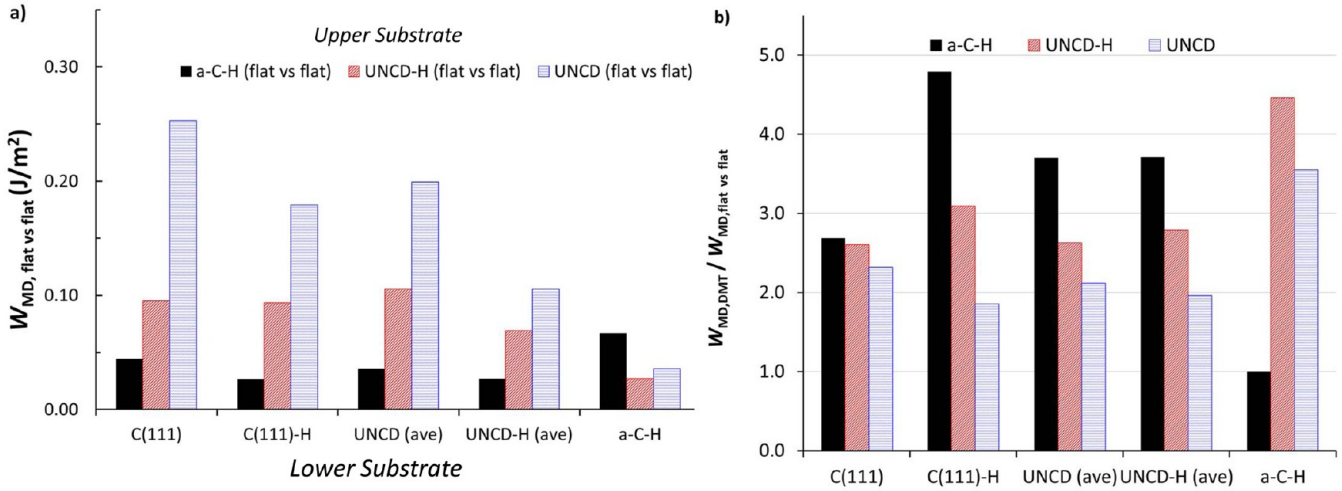

Figure 4. (a) Work of adhesion values ($W_{MD,flat\ vs\ flat}$) calculated by integrating the force curves generated from the interactions of the upper substrate (legend) with the lower substrate (x axis). (b) Comparison of the work of adhesion values calculated from tip−substrate interactions and the DMT equation ($W_{MD,DMT}$) with those calculated from the interaction of two infinitely flat substrates ($W_{MD,flat\ vs\ flat}$). The legend indicates the tip or upper substrate material.

the UNCD(001) (Figure 3c) substrates. A lack of H-termination on the tip and the substrate can also lead to hysteresis in the force curve (Figure 2), as discussed above.

Differences in F_{adh} are observed for different contact locations on the UNCD substrates. In general, contact with the grain boundary yields the lowest value of F_{adh} followed by contact with the (111) and the (001) grains for all tips (Figure 3b−d). Notably, the a-C−H tip produces the least variation in F_{adh} as a function of the substrate contact point. Finally, it is instructive to compare F_{adh} values from contact with the C(111)−H and UNCD−H(111) substrates (Figure3a,d) because these surfaces should "look" approximately similar to the tip (which is smaller at the apex than the grains). This comparison reveals that F_{adh} is slightly larger for the C(111)−H substrate than for the UNCD−H(111) substrate for all tips, with the difference being most pronounced for the UNCD tip. The trend is less clear when considering the H-free substrates.

Discussion of Methods for Determining the Work of Adhesion. There are two commonly used techniques for determining the W between two materials using an AFM: (1) measuring the F_{po} between a tip and a flat substrate and using a continuum model that provides a relationship between F_{po} and W and (2) measuring values of a contact parameter (e.g., contact stiffness or frictional force) at different normal load values and then fitting the data to the same adhesive contact mechanics models. Most of these models assume that the adhesion force is occurring between a smooth paraboloidal tip and smooth flat substrate. For example, the DMT and the JKR models both describe the contact of linearly elastic, adhesive paraboloids. The JKR model is appropriate when the materials are compliant, the forces are short-range, and the adhesion is strong, while the DMT model applies to stiff materials with long-range forces and weak adhesion. The Maugis-Dugale transition model[3] unifies the JKR and DMT theories and describes intermediate behaviors.

The simplest method for calculating W is to use AFM experiments to measure F_{po}. The DMT model relates F_{po} to W for paraboloidal tips through the relation $F_{po} = -2\pi RW$. In the Maugis−Dugdale model, the transition between JKR- and DMT-like behavior is given by the parameter λ, where $\lambda < 0.1$ for the DMT limit and $\lambda > 5$ for the JKR limit.[39]

Given the high modulus of UNCD and diamond, the DMT model is expected to be applicable, but this may not be the case for the softer a-C−H. The Tabor parameter, μ_T, is related to λ via the relation $\lambda = 1.1570\mu_T$, where $\mu_T = ((RW^2)/(E_r^2 z_o^3))^{1/3}$, E_r is the reduced modulus, and z_o is the equilibrium separation of the two bodies.[39] Using the values of E_r = 303 GPa,[23] R = 2.5 nm, z_o = 0.16 nm (estimated from the simulated force curves), and W = 0.171 J/m^2 for the a-C−H tip and the C(111)−H substrate pair (estimated using the JKR model providing an upper bound value for μ_T) yields a Tabor parameter of 0.058 and a λ value of 0.067, which is below the 0.1 DMT cutoff. The calculation of the ratio of the uppermost load, chosen to be 20 nN, to the pull-off force, $\bar{L}$, where $\bar{L}$ = (load)/(πRW_{adh}), yields a value of 19.9 for the a-C−H tip-C(111)−H substrate pair. These values result in the simulations being located in the DMT region on the adhesion map of $\bar{L}$ versus λ.[40]

By these two measures, the application of the DMT equation to the simulated values of F_{adh} to calculate W is justified within the framework of continuum mechanics. Continuum theories also assume a semi-infinite substrate, which is not the case here. Contact area and lateral stiffness corrections are negligible when $a/D < 0.1$,[41] where a is the contact radius and D is the substrate thickness. When the simulated contact area is calculated at the same point as F_{adh}, a/D is <0.1. It should be noted, however, that predictions from recent MD simulations of nanoscale contacts can deviate significantly from the predictions of continuum mechanics contact models depending on the atomic details of the contacting surfaces.[11] The calculated values of W from F_{adh} and R = 2.5 nm are thus effective values based on the application of the continuum DMT model and will be designated as $W_{MD,DMT}$. Because of the straightforward relationship between F_{adh} and $W_{MD,DMT}$, the trends described above in F_{adh} also apply to $W_{MD,DMT}$.

Extracting the "True" Work of Adhesion from the Simulation Results. A true value of W must be extracted from the simulation to assess the accuracy of $W_{MD,DMT}$. W has been calculated using MD by subtracting the energy per unit area of the two atomically flat substrates in equilibrium with zero applied force from the energy per unit area of the two substrates at infinite separation (periodic boundary conditions in the lateral directions, i.e., effectively infinite slabs); the area

dx.doi.org/10.1021/la404342d | Langmuir 2014, 30, 2028−2037

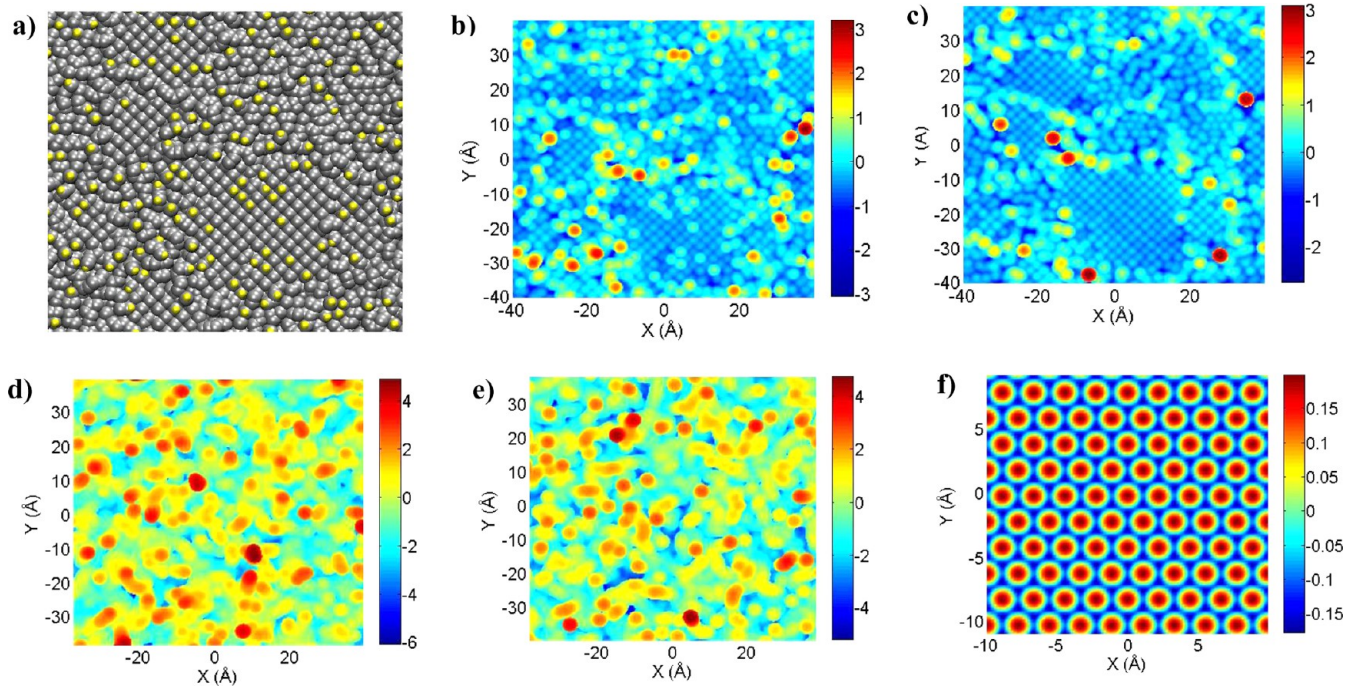

Figure 5. (a) Picture of the positions of atoms in the UNCD−H substrate. Gray and yellow spheres represent carbon and hydrogen atoms, respectively. Constant-force topographic maps of the top surface of the substrates under the tips. The UNCD−H, UNCD, a-C−H, a-C, and C(111)−H substrates are shown in b−f, respectively. The scale bar represents the distance (in angstroms) above the surface of the H_2 molecule used as the scanning probe. The average z distance has been subtracted from all of the z values.

refers to the area of the simulation cell.[11] Alternatively, two atomically flat substrates, with periodic boundary conditions, can be brought into normal contact, and a force curve can be generated. Integration of the force curve from the equilibrium separation to a large separation value yields an energy that is divided by the surface area to obtain W.[42] Simulations of the systems examined herein using both methods yielded approximately equal values of W. For simplicity, the latter method was used to calculate a true W (designated $W_{MD,flat\ vs\ flat}$) for the same material combinations examined in the tip-based simulations. The values of $W_{MD,flat\ vs\ flat}$ are shown in Figure 4a. Except for the a-C−H substrate, the flat substrates used to obtain $W_{MD,flat\ vs\ flat}$ were the same substrates as those used in the tip−substrate studies. In the flat versus flat simulations, the lengths of the simulation cells in the xy plane must be equal for both substrates. A new a-C−H substrate was needed with the same x and y dimensions as the UNCD and UNCD−H substrates.

Most of the trends observed in the $W_{MD,DMT}$ data are also apparent in the $W_{MD,flat\ vs\ flat}$ data (Figure 4a). For example, $W_{MD,flat\ vs\ flat}$ is always largest (or smallest) when the H-free UNCD (or a a-C−H) upper substrate is paired with any lower substrate except for a-C−H. The somewhat anomalous result of $W_{MD,flat\ vs\ flat}$ being larger for a-C−H paired with a-C−H than with UNCD or UNCD−H is likely due to the fact the a-C−H substrate is different from that used in tip−substrate simulations or the other flat versus flat simulations (see above).

Assessing the DMT Method of Calculating the Work of Adhesion. The simplicity of using F_{adh} to calculate W is appealing. Values of $W_{MD,DMT}$ calculated using F_{adh} and the DMT equation are compared to $W_{MD,flat\ vs\ flat}$ in Figure 4b. Because the simulations where $W_{MD,flat\ vs\ flat}$ is calculated involve a two-substrate geometry instead of a tip−substrate geometry, the substrates make contact at multiple points. Therefore, the values of $W_{MD,DMT}$ calculated from tips contacting the UNCD substrates are averaged over multiple contact points to facilitate comparison with the values of $W_{MD,flat\ vs\ flat}$

With the exception of the a-C−H versus a-C−H combination, the values of $W_{MD,flat\ vs\ flat}$ are smaller than those of $W_{MD,DMT}$ (Figure 4b) because of geometric differences in the systems. When the apex atoms of a finite tip come into contact with the substrate, they can relax laterally to allow a lower-energy configuration. In contrast, the asperities present on two flat surfaces with periodic boundary conditions imposed have a limited ability to relax laterally during contact because of the elastic constraints in both lateral directions. The finite nature of the tips also limits the length scale of the roughness in the contacting region to short wavelengths whereas contact using the two-substrate geometry spans roughness over many wavelengths.[11] Previous MD simulations that utilized Lennard-Jones potentials found that the apparent W increases as the contact area decreases.[11] It is interesting that the W values reported here, calculated using a more realistic potential than that used by Luan and Robbins, are consistent with their reported trends.

Variables Impacting the Work of Adhesion. Many factors are known to affect the magnitude of F_{adh}, including the roughness of the contacting surfaces[21,43] and surface termination.[14,44,45] Experiments,[43,46] simulations,[11,21,42,44] and models[7,45,47−51] have shown that increasing the surface roughness reduces the adhesion dramatically. The majority of the previous models and simulations have focused on the effect of substrate roughness on adhesion. Recently, the impact of tip roughness was examined by acquiring force curves in situ using transmission electron microscopy (TEM) combined with MD simulations and analytic models. The W value was shown to be exquisitely sensitive to tip roughness, down to the atomic limit.[21]

dx.doi.org/10.1021/la404342d | Langmuir 2014, 30, 2028−2037

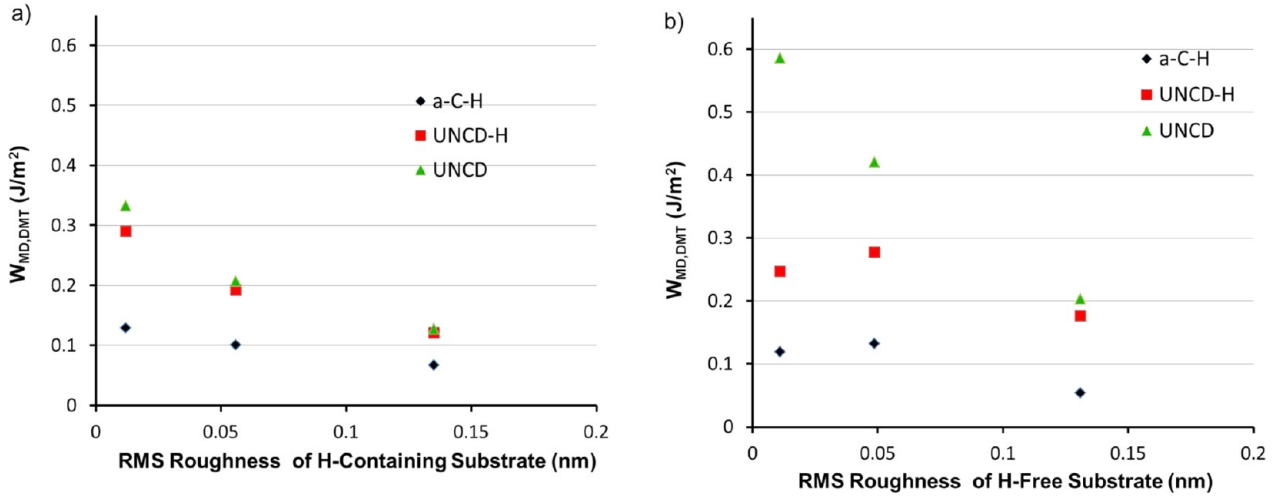

Figure 6. Work of adhesion calculated from F_{adh} using the DMT equation as a function of substrate roughness for (a) H-terminated and (b) H-free substrates. The legend indicates the tip identity. The roughness values for each substrate are listed in Table 1. Thus, Table 1 can be used to match the roughness values with the substrate identity.

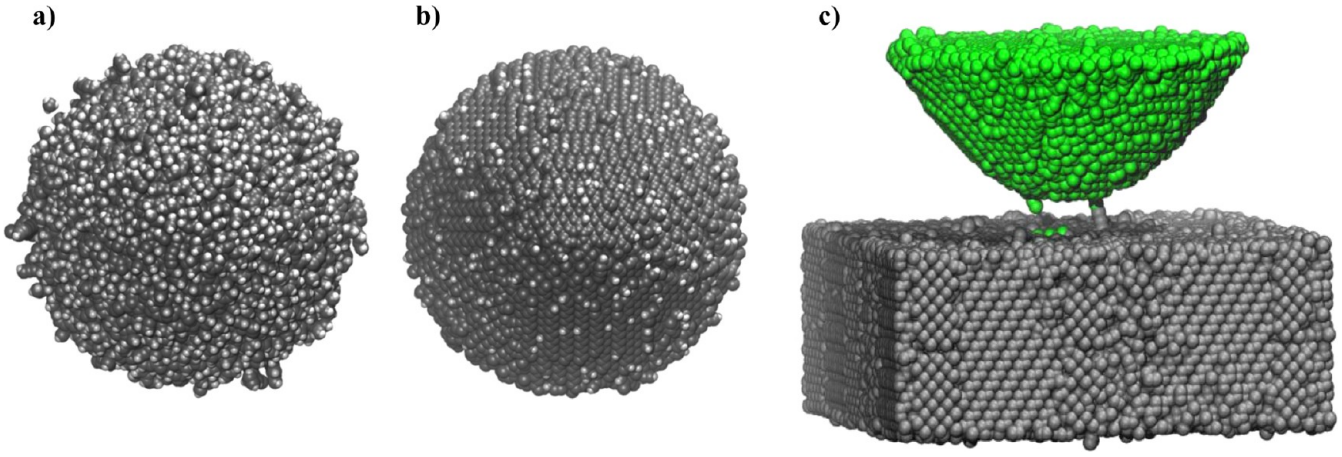

Figure 7. (a) a-C−H tip and (b) UNCD−H tip viewed along the z axis so that the apex of each tip is visible. (c) UNCD tip (green spheres) being pulled back from a UNCD substrate (gray spheres). Material from the tip has been transferred to the substrate, and bonding between the tip and the surface is apparent.

One convenient way to quantify the roughness of a substrate in MD simulations is to create a constant-force topographic plot. Such a plot can be created by orienting a "probe" molecule (or atom) perpendicular to the substrate surface and adjusting the distance of the molecule from the substrate to maintain a constant force as the molecule is rastered in x and y. The distance of the probe above the substrate where the force is constant at each x−y position is used to create a topographic map. Geometric features on the surface of the substrate that interact with the probe are apparent in topographic distance maps created in this way. For example, diamond grains and grain boundaries are apparent in both the geometric (Figure 5a) and constant force topographic images created with an H_2 molecule probe (Figure 5b) of the UNCD−H substrate. The 2D grid of distances can be used to calculate the effective root-mean-square (rms) roughness and the surface roughness power spectrum[52] of each substrate (Table 1). It is worth noting that an H_2 molecule was selected as the probe to raster over the surfaces because its small size allows for surface features to be resolved clearly. H-atom probes lead to approximately the same roughness values whereas the larger C-atom probes lead to slightly lower values of roughness with the same qualitative trends.

The diamond substrates have the smallest roughness values, followed by the UNCD and then the amorphous substrates. The H-terminated substrates are slightly rougher than their H-free counterparts. Because the same tip was used to contact each substrate, the effect of substrate roughness on $W_{MD,DMT}$ can be determined for each tip (Figure 6). The H-terminated and H-free substrates have been plotted separately (Figure 6a,b) to differentiate between surface roughness and H-termination effects. The values of $W_{MD,DMT}$ for the UNCD and UNCD−H tips are approximately equal on the rough a-C−H substrate (Figure 6a) and increase in nearly the same way as the substrate roughness decreases when the substrate is H-terminated. Differences in adhesion become more pronounced for these two tips as the roughness decreases to atomic corrugation on the C(111)−H substrate. On atomically smooth diamond, adhesion differences arises from the small amount of H termination (which alters the alignment and the roughness slightly) on the UNCD−H tip (Figure 7b) compared to that on the UNCD tip. Increasing the roughness of the substrate masks the small differences in adhesion as a result of the low levels of

dx.doi.org/10.1021/la404342d | Langmuir 2014, 30, 2028−2037

H termination on the tip. $W_{MD,DMT}$ of the a-C−H tip increases as the substrate roughness decreases, although not as markedly (Figure 6a). Removing H termination from the substrates causes a divergence in the values of $W_{MD,DMT}$ for the UNCD and UNCD−H tips (Figure 6b) as the roughness is reduced to atomic corrugation. Here, the behaviors of the UNCD−H and a-C−H tip are similar, although the values of $W_{MD,DMT}$ are lower for the a-C−H tip.

Recent TEM- and MD-based studies revealed that adhesion decreases by an order of magnitude as the roughness of the tip increases from atomic corrugation to an rms roughness of 0.5 nm.[21] Two-dimensional profiles of the tips were used to extract an approximate value of the rms roughness (denoted as 2D-RMS roughness) of the a-C−H (referred to as a DLC−H tip in Jacobs et al.[21]) and the UNCD−H tip used here. The a-C−H tip and the UNCD−H tip have comparable 2D rms roughness values of 0.033 and 0.031 nm, respectively. Using a 3D tip profile generated with an H-atom probe, the roughnesses of the a-C−H and UNCD−H tips are 0.136 and 0.085 nm, respectively. The power spectra of the two tips also have differences on the order of small wavelengths. The smoother UNCD−H tip has a larger value of $W_{MD,DMT}$ than the a-C−H tip regardless of the substrate being contacted (Figure 6a,b). Previous MD simulations examined the adhesion of a fully H-terminated diamond countersurface (C(111)−H with a 1 × 1 monolayer of H) with C(111) substrates with various levels of H termination.[42] The alignment of atoms on opposing substrates was shown to influence W, and the values can differ by as much as 0.1 J/m^2 as a function of surface alignment for substrates with atomic corrugation. The (111) grain at the apex of the UNCD−H tip (Figure 7b) makes it more sensitive to alignment issues with the substrate than the a-C−H tip (Figure 7a), which makes incommensurate contact with the substrate. Previous simulations found that the minimum adhesion occurred for a H coverage of between 20 and 30% for a monolayer.[42] The H-termination procedure did not produce a high level of H termination on the UNCD−H tip (Figure 7b), and the different levels of H termination of the UNCD−H and a-C−H tips (Figure 7) also contribute to the adhesion differences observed with these tips on the same substrate. Lastly, the divergence of $W_{MD,DMT}$ values for the UNCD and the UNCD−H tips on the atomically smooth, H-free substrates is due to the incomplete H termination of the UNCD−H tip.

Additional simulations of the adhesion between two diamond substrates reveal that when both substrates lack H termination the largest value of W is obtained when terminal C atoms on both diamond surfaces are aligned with each other as a result of the potential for C−C bond formation. Thus, W is between 1.2 to 1.6 times larger when self-mated C(111) surfaces are brought into contact than when one diamond surface has hydrogen termination depending upon the alignment of the surfaces. This causes the large value of $W_{MD,DMT}$ measured whenever the UNCD tip contacts the H-free surfaces (Figure 6b).

A critical factor that affects the experimental determination of F_{po} is the formation of chemical bonds between the tip and the substrate. Because it is not possible to determine the full extent of chemical-bond formation during the generation of AFM force curves, the effect of chemical-bond formation on F_{po} when the tip is separated from the sample is not fully quantified. In contrast, MD simulations reveal specific instances of bond formation between some tips and substrates. For example, when the UNCD tip is brought into contact with both the C(111) and the UNCD substrates, chemical bonds between the tip and the substrate result because the unsaturated C atoms on both surfaces allow for tip−substrate chemical bonds to form readily (Figure 7c). These chemical bonds increase the force required to separate the tip from the substrate; therefore, pulling back the UNCD tip from both substrates results in significant hysteresis in the force curves (Figure 2c,d). The sharp relaxations seen in the retraction portion of these force curves correspond to the progressive severing of these chemical linkages. The presence of H on the substrates prevents the formation of chemical bonds, and there is no hysteresis in the force curves (Figure 2a,b).

In the simulations where hysteresis occurs during pull-back, long chains of carbon atoms are formed between the tip and the substrate (Figure 7c), which eventually break when significant force is applied. Recently, it has been shown that the short cutoff distance of the REBO potential causes the force required to break covalent bonds to be significantly larger than that predicted by DFT calculations.[53] Pastewka et al. added a screening function to the REBO potential (REBO+S) that increased the interaction range of the potential. As a result, the REBO+S potential is able to reproduce the force required to break carbon−carbon bonds predicted by DFT calculations. Although conclusions about the quantitative value of the forces required to separate the tip and the substrate cannot be gleaned from the simulations presented here, the simulations do reveal the qualitative processes that occur when the H-free tip−substrate pairs come into contact.

There are several examples in the literature of H termination of hydrocarbon materials reducing the adhesion between nominally flat surfaces.[42] The simulations presented herein reveal that the W for tip−substrate contact are strongly affected not only by the H termination of the substrate and tip but also by the alignment of the tip and substrate and by the tip and substrate roughness. AFM has been used to measure the adhesion between a tungsten carbide tip and single-crystal diamond and UNCD substrates before and after H termination.[22] For both substrate materials, H termination was found to reduce the W value These simulations show that even a small amount of H termination on the tip can reduce the adhesion of the tip and an H-terminated sample if the sample is atomically smooth. As the roughness of the substrate increases, this effect is mitigated. In most cases, the H termination of the substrates reduces the W regardless of the roughness of the substrate. These simulations also demonstrate that even for small tips, crystalline structures at the apex of the tip can lead to alignment with ordered substrates. For both H-terminated and H-free substrates, the tip that makes incommensurate contact (a-C−H) (which is also the roughest tip) has the smallest W value regardless of the substrate.

The values of W obtained from the interaction of two infinitely flat surfaces are consistently lower than those calculated using the DMT equation and F_{adh}. Finite element simulations of contact between self-affine surfaces have shown that the distribution of contact sizes follows a power law for self-affine surfaces. However, introducing both small-scale and large-scale cutoffs into the wavelengths alters this behavior. Thus, it is not surprising that the W values calculated from the two methods used here with different geometries are not equivalent.

For all of the tips, the values of $W_{MD,DMT}$ when contact is made with the UNCD(001) surface are slightly larger than the values obtained when contact is made with the UNCD(111)

dx.doi.org/10.1021/la404342d | Langmuir 2014, 30, 2028−2037

surface for both H-terminated and H-free substrates. This effect has been observed in AFM experiments of an H-terminated amorphous carbon tip contacting the (001)(2 × 1)−H and the (111)(1 × 1)−H terraces of microcrystalline diamond.[23] The measured adhesion of the (001)(2 × 1)−H surface was 78−150% larger than the measured adhesion of the (111)(1 × 1)−H surface. This was thought to be due to larger electrostatic interactions caused by the increased polarization of the C−CH and C−H bonds on the (001)(2 × 1)−H surface compared to that on the (111) surface.[42] The relatively small increase in adhesion between the UNCD(001) surface and the tip compared to the UNCD(111) surface calculated here is due to alignment effects rather than electrostatic interactions. Thus, it is likely that both the alignment of the tip and sample atoms and electrostatic interactions contributed to the adhesion differences observed experimentally.

SUMMARY

Values of W were calculated from MD simulations of force curves between tips and substrates and between flat-substrate pairs. Differences as a function of tip/substrate material identity, H termination, contact point, and tip/substrate roughness have been elucidated. For all tip−substrate pairs examined, $W_{MD,DMT}$ (the W calculated by applying continuum contact mechanics to the adhesive force F_{adh}) increases with decreasing roughness of the substrate for both H-terminated and H-free substrates, as expected. For H-terminated substrates, rougher tips that make incommensurate contact with the substrate have the lowest $W_{MD,DMT}$, with the difference in adhesion compared to tips that make commensurate contact growing as the substrate becomes smoother. Even a small amount of H termination on crystalline tips can reduce the adhesion (compared to an H-free tip) if the tip is atomically smooth and the substrate is H-terminated. As the roughness of the substrate increases, this effect is mitigated. Removing H from the substrate results in an increased dependence of $W_{MD,DMT}$ on the substrate roughness (i.e., a-C−H tip), except when there is a small amount of hydrogen termination on the tip. This is because the adhesion between H-terminated surfaces is not a monotonic function of the amount of hydrogen termination.[42] Lastly, values of $W_{MD,DMT}$ obtained from tip−substrate contact using the DMT model were found to be approximately 2−5 times larger than values calculated from the interaction of the same substrate pairs in nominally flat versus flat geometries. This is likely due to the fact that geometric constraints do not allow for significant relaxation when two surfaces come into contact compared to tip−substrate contact and the fact that the finite size of the tip limits the wavelengths of roughness.

AUTHOR INFORMATION

Corresponding Author

*E-mail: jah@usna.edu.

Author Contributions

K.E.R. and P.L.K. contributed equally to this work.

Notes

The authors declare no competing financial interest.

ACKNOWLEDGMENTS

K.E.R. and P.L.K. acknowledge partial support from the AFOSR (contract number F1ATA00130G001) and the U.S. Naval Academy Research Office. K.E.R. and J.A.H. acknowledge partial support from the NSF (contract numbers N0016108WENA056, IAA 1129630, and CMMI 1200011). R.W.C. and K.T.T. acknowledge support from the NSF (CMMI 1200019).

REFERENCES

(1) Johnson, K. L.; Kendall, K.; Roberts, A. D. Surface Energy and Contact of Elastic Solids. *Proc. R. Soc. London, Ser. A* **1971**, *324*, 301−313.
(2) Derjaguin, B. V.; Muller, V. M.; Toporov, Y. P. Effect of Contact Deformations on Adhesion of Particles. *J. Colloid Interface Sci.* **1975**, *53*, 314−326.
(3) Maugis, D. Adhesion of Spheres - The JKR-DMT Transition Using a Dugdale Model. *J. Colloid Interface Sci.* **1992**, *150*, 243−269.
(4) Maugis, D. Extension of the Johnson-Kendall-Roberts Theory of the Elastic Contact of Spheres to Large Contact Radii. *Langmuir* **1995**, *11*, 679−682.
(5) Greenwood, J. A. Adhesion of Small Spheres. *Philos. Mag.* **2009**, *89*, 945−965.
(6) Yao, H. M.; Ciavarella, M.; Gao, H. J. Adhesion Maps of Spheres Corrected for Strength Limit. *J. Colloid Interface Sci.* **2007**, *315*, 786−790.
(7) Persson, B. N. J. Nanoadhesion. *Wear* **2003**, *254*, 832−834.
(8) Gao, H. J.; Yao, H. M. Shape Insensitive Optimal Adhesion of Nanoscale Fibrillar Structures. *Proc. Natl. Acad. Sci. U.S.A.* **2004**, *101*, 7851−7856.
(9) Grierson, D. S.; Liu, J. J.; Carpick, R. W.; Turner, K. T. Adhesion of Nanoscale Asperities with Power-Law Profiles. *J. Mech. Phys. Solids* **2013**, *61*, 597−610.
(10) Luan, B. Q.; Robbins, M. O. The Breakdown of Continuum Models for Mechanical Contacts. *Nature* **2005**, *435*, 929−932.
(11) Luan, B. Q.; Robbins, M. O. Contact of Single Asperities with Varying Adhesion: Comparing Continuum Mechanics to Atomistic Simuations. *Phys. Rev. E* **2006**, *74*, 026111-1−026111-17.
(12) Erdemir, A.; Donnet, C. Tribology of Diamond-Like Carbon Films: Recent Progress and Future Prospects. *J. Phys. D* **2006**, *39*, R311−R327.
(13) Casiraghi, C.; Robertson, J.; Ferrari, A. C. Diamond-Like Carbon for Data and Beer Storage. *Mater. Today* **2007**, *10*, 44−53.
(14) Auciello, O.; Pacheco, S.; Sumant, A. V.; Gudeman, C.; Sampath, S.; Datta, A.; Carpick, R. W.; Adiga, V. P.; Zurcher, P.; Ma, Z.; Yuan, H. C.; Carlisle, J. A.; Kabius, B.; Hiller, J.; Srinivasan, S. Are Diamonds a MEMS' Best Friend? *IEEE Microwave Mag.* **2007**, *8*, 61−75.
(15) Auciello, O.; Birrell, J.; Carlisle, J. A.; Gerbi, J. E.; Xiao, X.; Peng, B.; Espinosa, H. D. Materials Science and Fabrication Processes for a New MEMS Technology Based on Ultrananocrystalline Diamond Thin Films. *J. Phys.: Condens. Matter* **2004**, *16*, 539−552.
(16) Liu, J.; Grierson, D. S.; Moldovan, N.; Notbohm, J.; Li, S.; Jaroenapibal, P.; O'Connor, S. D.; Sumant, A. V.; Neelakantan, N.; Carlisle, J. A.; Turner, K. T.; Carpick, R. W. Preventing Nanoscale Wear of Atomic Force Microscopy Tips Through the Use of Monolithic Ultrananocrystalline Diamond Probes. *Small* **2010**, *6*, 1140−1149.
(17) Kim, K. H.; Moldovan, N.; Ke, C.; Espinosa, H. D.; Xiao, X.; Carlisle, J. A.; Auciello, O. Novel Ultrananocrystalline Diamond Probes for High-Resolution Low-Wear Nanolithographic Techniques. *Small* **2005**, *1*, 912−912.
(18) Sekaric, L.; Parpia, J. M.; Craighead, H. G.; Feygelson, T.; Houston, B. H.; Butler, J. E. Nanomechanical Resonant Structures in Nanocrystalline Diamond. *Appl. Phys. Lett.* **2002**, *81*, 4455−4457.
(19) Hutchinson, A. B.; Truitt, P. A.; Schwab, K. C.; Sekaric, L.; Parpia, J. M.; Craighead, H. G.; Butler, J. E. Dissipation in Nanocrystalline-Diamond Nanomechanical Resonators. *Appl. Phys. Lett.* **2004**, *84*, 972−974.
(20) Carlisle, J. A.; Auciello, O. Ultrananocrystalline Diamond. Properties and Applications in Biomedical Devices. *Electrochem. Soc. Interface* **2003**, *12*, 28−31.

(21) Jacobs, T. D.; Ryan, K. E.; Keating, P. L.; Grierson, D. S.; Lefever, J. A.; Turner, K. T.; Harrison, J. A.; Carpick, R. W. The Effect of Atomic-Scale Roughness on the Adhesion of Nanoscale Asperities: A Combined Simulation and Experimental Investigation. *Tribol. Lett.* **2013**, *50*, 81−93.
(22) Sumant, A. V.; Grierson, D. S.; Gerbi, J. E.; Carlisle, J. A.; Auciello, O.; Carpick, R. W. Surface Chemistry and Bonding Configuration of Ultrananocrystalline Diamond Surfaces and Their Effects on Nanotribological Properties. *Phys. Rev. B* **2007**, *76*, 235429-1−235429-11.
(23) Gao, G. T.; Cannara, R. J.; Carpick, R. W.; Harrison, J. A. Atomic-Scale Friction on Diamond: A Comparison of Different Sliding Directions on (001) And (111) Surfaces Using MD and AFM. *Langmuir* **2007**, *23*, 5394−5405.
(24) Knippenberg, M. T.; Mikulski, P. T.; Ryan, K. E.; Stuart, S. J.; Gao, G. T.; Harrison, J. A. Bond-Order Potentials with Split-Charge Equilibration: Application To C-, H-, and O-Containing Systems. *J. Chem. Phys.* **2012**, *136*, 164701-1−164701-11.
(25) van Duin, A. C. T.; Dasgupta, S.; Lorant, F.; Goddard, W. A. ReaxFF: A Reactive Force Field for Hydrocarbons. *J. Phys. Chem. A* **2001**, *105*, 9396−9409.
(26) Erdemir, A.; Donnet, C. Tribology of Diamond, Diamond-Like Carbon, and Related Films. In *Modern Tribology Handbook*; Bhushan, B., Ed.; CRC Press: Boca Raton, FL, 2001; Vol. 2, pp 871−908.
(27) Bilek, M. M. M.; McKenzie, D. R.; McCulloch, D. G.; Goringe, C. M. Ab Initio Simulation of Structure in Amorphous Hydrogenated Carbon. *Phys. Rev. B* **2000**, *62*, 3071−3077.
(28) Glosli, J. N.; Ree, F. H. Liquid-Liquid Phase Transformation in Carbon. *Phys. Rev. Lett.* **1999**, *82*, 4659−4662.
(29) Marks, N. Modelling Diamond-Like Carbon with the Environment-Dependent Interaction Potential. *J. Phys.: Condens. Matt.* **2002**, *14*, 2901−2927.
(30) Marks, N. A.; McKenzie, D. R.; Pailthorpe, B. A.; Bernasconi, M.; Parrinello, M. Microscopic Structure of Tetrahedral Amorphous Carbon. *Phys. Rev. Lett.* **1996**, *76*, 768−771.
(31) Adelman, S. A.; Doll, J. D. Generalized Langevin Equation Approach for Atom/Solid-Surface Scattering: General Formulation of Classical Scattering off Harmonic Solids. *J. Chem. Phys.* **1976**, *64*, 2375−2388.
(32) Gruen, D. M. Nanocrystalline Diamond Films. *Annu. Rev. Mater. Sci.* **1999**, *29*, 211−259.
(33) Gruen, D. M.; Krauss, A. R.; Zuiker, C. D.; Csencsits, R.; Terminello, L. J.; Carlisle, J. A.; Jimenez, I.; Sutherland, D. G. J.; Shuh, D. K.; Tong, W.; Himpsel, F. J. Characterization of Nanocrystalline Diamond Films by Core-Level Photoabsorption. *Appl. Phys. Lett.* **1996**, *68*, 1640−1642.
(34) Philip, J.; Hess, P.; Feygelson, T.; Butler, J. E.; Chattopadhyay, S.; Chen, K. H.; Chen, L. C. Elastic, Mechanical, And Thermal Properties of Nanocrystalline Diamond Films. *J. Appl. Phys.* **2003**, *93*, 2164−2171.
(35) Stuart, S. J.; Tutein, A. B.; Harrison, J. A. A Reactive Potential for Hydrocarbons with Intermolecular Interactions. *J. Chem. Phys.* **2000**, *112*, 6472−6486.
(36) LAMMPS Molecular Dynamics Simulator. http://lammps.sandia.gov/index.html.
(37) Harrison, J. A.; Schall, J. D.; Knippenberg, M. T.; Gao, G.; Mikulski, P. T. Elucidating Atomic-Scale Friction using MD and Specialized Analysis Techniques. *J. Phys.: Condens. Matter* **2008**, *20*, 354009−1−354009−15.
(38) Cappella, B.; Dietler, G. Force-Distance Curves by Atomic Force Microscopy. *Surf. Sci. Rep.* **1999**, *34*, 1−104.
(39) Grierson, D. S.; Flater, E. E.; Carpick, R. W. Accounting for the JKR-DMT transition in adhesion and friction measurements with atomic force microscopy. *J. Adhes. Sci. Technol.* **2005**, *19*, 291−311.
(40) Johnson, K. L.; Greenwood, J. A. An Adhesion Map for the Contact of Elastic Spheres. *J. Colloid Interface Sci.* **1997**, *192*, 326−333.
(41) Johnson, K. L. *Contact Mechanics*; Cambridge University Press: Cambridge, U.K., 1985.
(42) Piotrowski, P. L.; Cannara, R. J.; Gao, G. T.; Urban, J. J.; Carpick, R. W.; Harrison, J. A. Atomistic Factors Governing Adhesion between Diamond, Amorphous Carbon and Model Diamond Nanocomposite Surfaces. *J. Adhes. Sci. Technol.* **2010**, *24*, 2471−2498.
(43) Fuller, K.; Tabor, D. Effect of Surface-Roughness on Adhesion of Elastic Solids. *Proc. R. Soc. London, Ser. A* **1975**, *345*, 327−342.
(44) Mulakaluri, N.; Persson, B. N. J. Adhesion between Elastic Solids with Randomly Rough Surfaces: Comparison of Analytical Theory with Molecular-Dynamics Simulations. *Europhys. Lett.* **2011**, *96*, 66003-1−66003-6.
(45) Maugis, D. On the Contact and Adhesion of Rough Surfaces. *J. Adhes. Sci. Technol.* **1996**, *10*, 161−175.
(46) DelRio, F. W.; De Boer, M. P.; Knapp, J. A.; Reedy, E. D.; Clews, P. J.; Dunn, M. L. The Role of van der Waals Forces in Adhesion of Micromachined Surfaces. *Nat. Mater.* **2005**, *4*, 629−634.
(47) Greenwood, J. A.; Williamson, J. Contact of Nominally Flat Surfaces. *Proc. R. Soc. London, Ser. A* **1966**, *295*, 300−319.
(48) Katainen, J.; Paajanen, M.; Ahtola, E.; Pore, V.; Lahtinen, J. Adhesion as an Interplay between Particle Size and Surface Roughness. *J. Colloid Interface Sci.* **2006**, *304*, 524−529.
(49) Rabinovich, Y. I.; Adler, J. J.; Ata, A.; Singh, R. K.; Moudgil, B. M. Adhesion between Nanoscale Rough Surfaces - I. Role of Asperity Geometry. *J. Colloid Interface Sci.* **2000**, *232*, 10−16.
(50) Rabinovich, Y. I.; Adler, J. J.; Ata, A.; Singh, R. K.; Moudgil, B. M. Adhesion between Nanoscale Rough Surfaces - II. Measurement and Comparison with Theory. *J. Colloid Interface Sci.* **2000**, *232*, 17−24.
(51) Rumpf, H. *Particle Technology*; Chapman and Hall: London, 1990.
(52) Persson, B. N. J.; Albohr, O.; Tartaglino, U.; Volokitin, A. I.; Tosatti, E. On the Nature of Surface Roughness with Application to Contact Mechanics, Sealing, Rubber Friction and Adhesion. *J. Phys.: Condens. Matter* **2005**, *17*, R1−R62.
(53) Pastewka, L.; Pou, P.; Perez, R.; Gumbsch, P.; Moseler, M. Describing Bond-Breaking Processes by Reactive Potentials: Importance of an Environment-Dependent Interaction Range. *Phys. Rev. B* **2008**, *78*, 161402-1−161402-4.